Tuning electronic transport via hepta-alanine peptides junction by tryptophan doping

Cunlan Guo[a,b,1], Xi Yu[a,1], Sivan Refaely-Abramson[a], Lior Sepunaru[a,b], Tatyana Bendikov[c], Israel Pecht[d], Leeor Kronik[a], Ayelet Vilan[a], Mordechai Sheves[b], and David Cahen[a,2]

[a]Department of Materials and Interfaces, Weizmann Institute of Science, Rehovot, Israel 76100; [b]Department of Organic Chemistry, Weizmann Institute of Science, Rehovot, Israel 76100; [c]Department of Chemical Research Support, Weizmann Institute of Science, Rehovot, Israel 76100; and [d]Department of Immunology, Weizmann Institute of Science, Rehovot, Israel 76100

Edited by Harry B. Gray, California Institute of Technology, Pasadena, CA, and approved July 29, 2016 (received for review April 28, 2016)

Charge migration for electron transfer via the polypeptide matrix of proteins is a key process in biological energy conversion and signaling systems. It is sensitive to the sequence of amino acids composing the protein and, therefore, offers a tool for chemical control of charge transport across biomaterial-based devices. We designed a series of linear oligoalanine peptides with a single tryptophan substitution that acts as a "dopant," introducing an energy level closer to the electrodes' Fermi level than that of the alanine homopeptide. We investigated the solid-state electron transport (ETp) across a self-assembled monolayer of these peptides between gold contacts. The single tryptophan "doping" markedly increased the conductance of the peptide chain, especially when its location in the sequence is close to the electrodes. Combining inelastic tunneling spectroscopy, UV photoelectron spectroscopy, electronic structure calculations by advanced density-functional theory, and dc current–voltage analysis, the role of tryptophan in ETp is rationalized by charge tunneling across a heterogeneous energy barrier, via electronic states of alanine and tryptophan, and by relatively efficient direct coupling of tryptophan to a Au electrode. These results reveal a controlled way of modulating the electrical properties of molecular junctions by tailor-made "building block" peptides.

oligopeptide | electron transport | self-assembled monolayer | inelastic electron tunneling spectroscopy | doping

Electron transfer (ET) processes taking place between prosthetic groups across the polypeptide matrices of proteins (1–3) have been extensively explored by, e.g., time-resolved photolysis (4, 5), pulse radiolysis (6, 7), scanning tunneling microscopy (8, 9), electrochemical methods (10–12), and by theoretical studies (13–16). The surprisingly fast and efficient ET over considerable distances (up to ∼25 Å) (17) via peptide matrices in proteins suggests possible development of peptide- and protein-based bioelectronics with diverse functionality and relative ease of modification (18, 19). Studying electron transport (ETp) via solid-state molecular junctions represents an approach, bridging the study of basic ET-related phenomena and electronic devices, where measuring ET rates as a function of an electrochemical driving force is replaced by measuring current across molecular junctions as a function of an applied electrical voltage (20). Combining the concepts and methods of molecular electronics such as current–voltage (I-V) line-shape analysis (21, 22), temperature-dependent measurements (23, 24), and electronic spectroscopy techniques (25–27) may yield new insights into the mechanism of ETp across the peptide matrix of proteins (28–30) and pave the road to peptide- and protein-based electronic devices for switching, rectification, and memory (18, 31).

ETp via homopeptides has been investigated, probing the roles of specific amino acid residues, their protonation, and secondary structure (29, 32). Synthetic heteropeptides with defined composition and sequence are a next step in developing model systems for investigating protein ETp. The heteropeptide model also helps in studying the properties of individual amino acids within a peptide. Tryptophan (Trp, W) and alanine (Ala, A) are amino acids with a large difference in ionization potential (IP) (15). In an earlier study we demonstrated that ETp across Trp with its conjugated indole side group is more efficient than through Ala with its saturated methyl side group (32). That result agrees with the known effects of Trp on ET in nature (33–35), such as acting as a redox-active "relay station" in hopping transport (19, 33, 36, 37), and can be attributed to the indole, on the frontier orbitals of the peptide, i.e., a decreased highest occupied molecular orbital–lowest unoccupied molecular orbital gap, because of lower ionization potential and increased electron affinity.

Here, we report a study of a series of heteropeptides, where one Trp residue "dopes" the hepta-alanine at different locations (Fig. 1*A*). We fabricated dry, solid-state electronic junctions with these peptides confined between two gold electrodes. The temperature-dependent I-V characteristics via these peptides were investigated and inelastic tunneling spectroscopy (IETS) at ∼10 K provided vibrational information on the chemical groups involved in the transport. Combining UV photoelectron spectroscopy (UPS) and high-level density-functional theory (DFT) calculations, we observed that the peptides' heterogeneous sequence (by doping the Ala-peptides with Trp) affects the ETp via the peptide junctions, including peptide–electrode coupling.

Results and Discussion

We used four different peptides: hepta-Ala (7A) and three hepta-peptides composed of six Ala and a single Trp located at the N terminus (W-1), the peptide's middle (W-4), or at the C terminus

Significance

Charge transport is a process that is central to redox reactions, enzyme catalysis, and electronics. Integrating biomolecules into electronic devices provides a route to using natural evolution in artificial technology. Charge transport across biomolecules depends on the molecular structure and molecule–electrode contacts. We show that "doping" (7-alanine) peptide-based devices by one tryptophan enhances transport ≥10-fold, regardless of tryptophan position, a result that can be described by super-exchange-mediated tunneling through multiple sites. Remarkably, close physical proximity of tryptophan to a gold electrode further enhances transport, showing how crucial electronic coupling to the electrode is. Our results provide insight into charge transfer through biomolecules and offer a strategy for tailored bioelectronics by mix-and-match amino acid building blocks.

Author contributions: C.G., L.S., I.P., L.K., A.V., M.S., and D.C. designed research; C.G., X.Y., S.R.-A., L.S., T.B., and A.V. performed research; C.G., X.Y., S.R.-A., L.S., T.B., I.P., L.K., A.V., M.S., and D.C. analyzed data; and C.G., X.Y., I.P., L.K., A.V., M.S., and D.C. wrote the paper.

The authors declare no conflict of interest.

This article is a PNAS Direct Submission.

[1]C.G. and X.Y. contributed equally to this work.

[2]To whom correspondence should be addressed. Email: david.cahen@weizmann.ac.il.

This article contains supporting information online at www.pnas.org/lookup/suppl/doi:10.1073/pnas.1606779113/-/DCSupplemental.

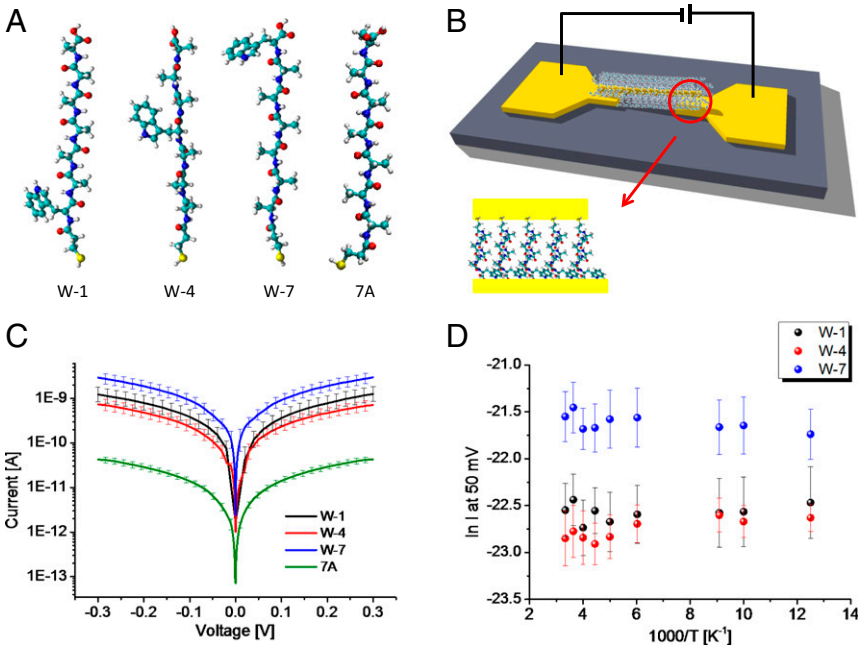

Fig. 1. Scheme of experimental setup and results of current–voltage measurements. (*A*) Structure of peptides used: W-1: MPA-WAAAAAA; W-4: MPA-AAAWAAA; W-7: MPA-AAAAAAW; 7A: MPA-AAAAAAA (A = alanine, W = tryptophan). MPA is attached at the peptides' N terminus. (*B*) Schematic drawing of Au–peptide–Au junction setup. A peptide monolayer-covered Au NW is suspended on top of two Au electrodes to form the closed circuit. (*C*) Current–voltage plots at 300 K for Au–peptide–Au junctions of W-1, W-4, W-7, and 7A. Each plot is the average of ∼20 curves. (*D*) Temperature-dependent currents at 50 mV measured as function of 1,000/T through W-1, W-4, and W-7.

(W-7). All peptides had a mercaptopropionic acid (MPA) covalently bound to their N terminus to allow chemisorption of the peptide to a gold surface via Au–S binding (Fig. 1*A*; see *SI Appendix*, section SI-6 for experimental details).

The electronic junctions of the four studied peptides were fabricated by electrophoretic trapping of a gold nanowire (NW) between macroscopic electrodes as demonstrated before (38). An MPA-modified peptide monolayer was self-assembled on the NWs before the trapping (Fig. 1*B*).

To characterize the structure and quality of the peptide monolayers, similar monolayers were prepared on up to 2-cm^2 Au substrates for polarization modulation–infrared reflection-absorption spectroscopy (PM-IRRAS) and ellipsometry measurements. PM-IRRAS showed the amide I and II modes at ∼1,668 and 1,542 cm^{-1}, in agreement with the presence of the peptide on the Au (39) (*SI Appendix*, Fig. S1 and Table S1). Similar optical thickness values (20–26 Å) were obtained for all three peptides with the Trp at different locations (*SI Appendix*, Table S2). These values are slightly below the ∼30-Å theoretical length of the peptide in totally extended conformation, indicating that in monolayers the peptides are somewhat tilted or have slightly crumpled conformations.

The current–voltage characteristics across different peptide junctions (Fig. 1*C*) were measured by applying a bias between macroscopic electrodes (Fig. 1*B*). The conductance via the junctions is found to vary as W-7 > W-1 ∼ W-4 >> 7A (see Fig. 1*A* for nomenclature). Conductance dramatically increases, by about an order of magnitude when a Trp substitutes one Ala. [We note that replacing partial aliphatic with an aromatic group in hydrocarbon chains did not significantly change the conductance (40).] Moreover, the conductance via the heteropeptides varies, depending on the Trp location in the sequence, i.e., with Trp next to the linker (W-1) the conductance is slightly higher than with Trp in the middle (W-4), whereas with the Trp at the C terminus (W-7) conductance is significantly higher than for the other heteropeptides.

Temperature-dependent ETp via the peptides was measured to shed light on the transport mechanism. No temperature dependence of the current at 50 mV was observed from 80 to 300 K (Fig. 1*D*). This behavior suggests that ETp is via tunneling for all of the examined peptides, viz., that the transported electrons are not trapped by/on the Trp.

To further investigate the nature of the ETp process, we performed IETS of the peptide junctions at even lower temperature (∼10 K) (Fig. 2). IETS is an all-electronic spectroscopy method that records the changes in current due to the interaction between charge and molecular vibrations (41). As such, it provides in situ information on the molecular chemical groups involved in the electronic transport (26, 27, 42), with the implicit assumption that the inelastic part of the tunneling process reflects the main transport path.

In IETS, the second derivative of the current (dI^2/d^2V) shows peaks at specific bias corresponding to the energy of the vibrational modes. As shown in Fig. 2, IETS peaks between 2,930 and 2,960 cm^{-1} are observed for all of the peptides. These correspond to the C–H stretching of the MPA linker and Ala CH_3 group. Peaks in the ∼1,400- and ∼1,500-cm^{-1} spectral regions are possibly due to CH_2/CH_3 wagging and scissoring (42) of the MPA linker's CH_2 and/or the Ala's CH groups. Most importantly, peaks at ∼1,580 cm^{-1} stem from C=C vibration within the Trp's indole ring (39). No peak at this position was observed for 7A. This result shows the involvement of the Trp's indole group in ETp for all of the heteropeptides, irrespective of Trp position in the peptide. The amides I and II do not appear in the peptide's IETS, in agreement with our earlier results (43). This is probably due to the perpendicular orientation of the amide bond, relative to the charge transport direction. This result is relevant to the question whether the inelastic (scattering) process is preferentially due to the molecule–electrode interface (44), or to all parts of the molecule that take part in charge transport (45). Our results seem to support the latter interpretation, because the C=C peak is observed for all Trp-containing peptides, regardless of Trp position, implying scattering by the indole when charges pass through the Trp.

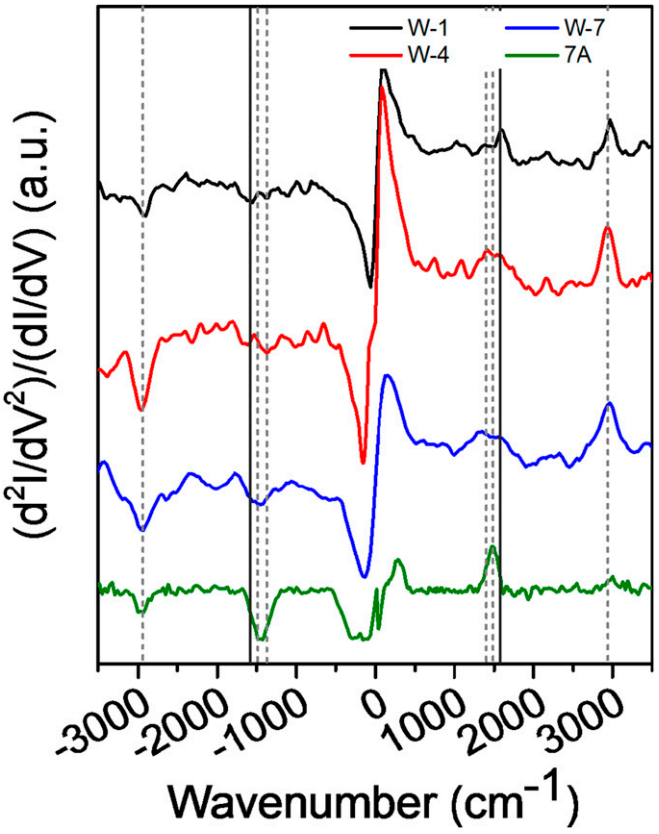

Fig. 2. IETS of W-1, W-4, W-7, and 7A measured at cryogenic temperature (~10 K), shown as second derivative of current (d^2I/dV^2) and normalized to conductance for baseline correction. The broken, light lines indicate the peaks. The characteristic C=C stretching of the indole residue of Trp (solid gray) is absent in 7A.

We propose that Trp doping affects the energy landscape of the peptide and therefore the charge transport across it. DFT-based transport calculations are very sensitive to level alignment issues (46) and more accurate theories would be prohibitively expensive here. Therefore, to assess if the presence of Trp affects the frontier molecular orbital energy levels of the whole peptide, we performed DFT calculations using an optimally tuned range-separated hybrid functional to evaluate the accurate detailed electronic structures of the peptides in the gas phase (32, 47–49). Unlike in standard DFT approximations the HOMO level from this approach corresponds to the negative of the ionization potential, −IP, a key parameter determining energy alignment for transport. DFT calculations reveal that replacing one Ala by a Trp in the original 7A peptides results in dramatic change of the peptide electronic structure (Fig. 3). The HOMO of 7A is localized on the MPA linker that binds the peptide to the electrode, and the deeper MO levels of the peptide are delocalized across the 7A chain. These can be assumed to dominate transport along the chain. In contrast, the HOMO levels of Trp-containing peptides are localized over the indole ring of the Trp, thus creating more heterogeneous electronic states for ETp via the doped, rather than via Ala-only peptides. With Trp, the HOMO levels are much higher than that of 7A (Figs. 3 and 4*A*), implying that the presence of Trp decreases the overall energy barrier for ETp. This is the main origin of the Trp doping effect accounting for the ~10-fold increase in conductance for doped peptides compared with the 7A (Fig. 1*C*).

The energy landscapes of the peptide monolayers were further examined by solid-state UPS to determine experimentally the work function and IP of each peptide monolayer on a Au surface. The IP values of the Trp-doped peptide monolayers are significantly smaller than for the Ala homopeptide (*SI Appendix*, Fig. S3*A*). This trend agrees with the gas-phase DFT calculations, although, as expected, the differences between IPs derived from UPS are smaller than the gas-phase DFT differences. Stabilization of energy levels upon adsorption (i.e., from gas-phase to surface-adsorbed species) is well-documented and attributed to surface polarization effects (50), dipole–dipole interactions between peptides in the monolayer (51, 52), and molecule–substrate charge rearrangement (53, 54). However, the work functions of the peptide monolayers on Au hardly change with Trp position (*SI Appendix*, Fig. S3*B*). This indicates that peptide–electrode interaction at the N terminus is mainly due to the MPA linker (54), and that Trp is not involved directly in energy alignment at that Au interface. Also, the dipole moment changes of the peptide with changing Trp position do not appear to affect this energy alignment.

Based on the above observations it is reasonable to assume that conduction via the heteropeptide junctions can be described by tunneling through an energy barrier that is heterogeneous. Actually, it has been observed for ET via a protein that "folded polypeptide matrices do not create a uniform barrier to electron tunneling" (17). In the pathway model for tunneling via proteins (14, 55, 56), the heterogeneous barrier is composed of superexchange-mediated transfer steps via distinct structural elements such as covalent and hydrogen bonds, and free space. A similar idea of "series tunneling" was recently applied to organic molecular junctions (57), where the heterogeneous states of alkyl- and phenyl groups of the molecule in the junction are modeled as series barriers [a Wentzel–Kramers–Brillouin model-based approximation (20)] or sites with different energies and coupling (superexchange). Within this conceptual frame, the seven amino acids as well as the linker can be viewed as subunits, acting in series (58), as shown schematically in Fig. 4*A*.

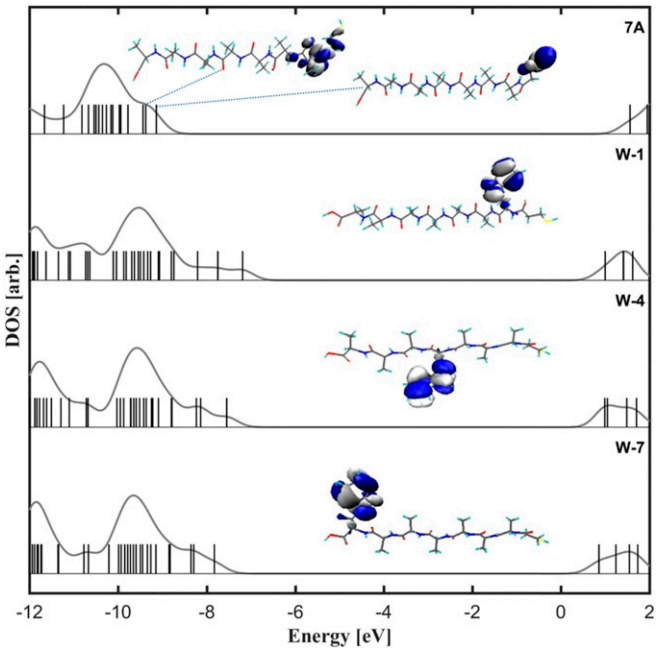

Fig. 3. Electronic structure calculations of W-1, W-4, and W-7 and their comparison with 7A. Zero energy corresponds to the vacuum level.

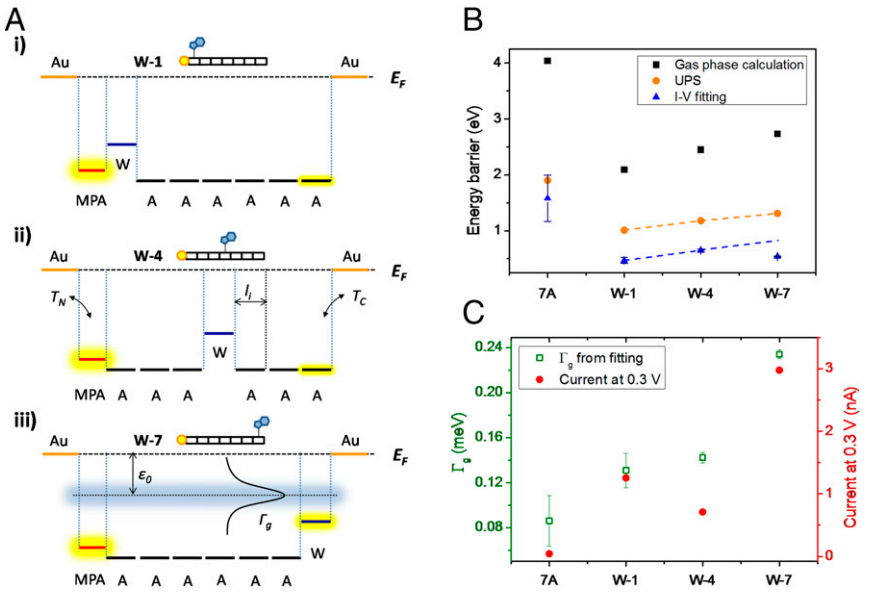

Fig. 4. Schemes of tunneling model for transport via generic peptides, and experimentally extracted transport parameter from fitting I-V curves to Eq. **2**. (*A*) Schematic energy level diagrams of W-1 (*A*, *i*), W-4 (*A*, *ii*), and W-7 (*A*, *iii*) as used in multistep models. E_F is the electrodes' Fermi level. The vertical direction is energy, and the horizontal axis is distance; *A*, *ii*, uses W-4 for a general illustration of the model expressed by Eq **1**; *A*, *iii*, does likewise with W-7 of Eq. **2**. In *A*, *iii*, the effective single level of the peptide bridge, ε_0, is shown as a dotted horizontal line, defining the effective energy barrier for tunneling; the Lorentzian curve represents the tunneling transmission probability related to Γ_g, the coupling. (*B*) Comparison of energy barrier heights for peptide–electrode(s) from gas-phase calculations of the free peptides (black squares, relative to −5.1 eV Au Fermi level), UPS measurements of peptide monolayers on Au (orange circles), and I-V curves of Au–peptide–Au junctions (blue triangles; for W-1, W-4, and W-7 the error bars are smaller than the triangular symbol). Dashed lines are guides to the eye and emphasize the difference for W-7 between the UPS and I-V fitting-derived energy barriers. (*C*) Comparison of trends for peptide–electrode coupling (Γ_g) (hollow green) and measured junction currents (solid red).

The low-bias current through a heterogeneous junction can be described as

$$I \propto T_C \cdot T_N \cdot \exp\left(\sum_{i=1}^{n}(-\beta_i l_i)\right), \qquad [1]$$

where β_i and l_i are the transport attenuation factor and length of individual subunits, respectively. T_N and T_C describe the coupling-dependent tunneling probability across the electrode/MPA linker and C terminus/electrode interfaces, respectively (compare Fig. 4 *A*, *ii* for a schematic illustration of the parameters of Eq. **1**) (57). Based on Eq. **1**, the higher conductance of W-doped alanine peptides can be understood by decreased attenuation upon doping, $\beta_W < \beta_A$, because of the $|E_F(Au) - E_{HOMO}|$ decrease (Figs. 3 and 4*A*). Assuming T_C and T_N do not change, $I_{W\text{-}4}/I_{7A}$ would correspond to β_W/β_A of ∼2.5/amino acid (or ∼0.7/Å) (see *SI Appendix*, section SI-5 for derivation). The observed similar currents via W-1 and W-4 (Fig. 1*C*) suggest that changing the sequence of the amino acids hardly affects the ETp efficiency in accordance with Eq. **1** (i.e., the $\beta_i l_i$ terms can be commutated). Our results thus suggest that the energy levels of the amino acids in these peptides are roughly independent, consistent with the similar density of states of these peptides (derived either from DFT computations, Fig. 3, or from UPS, Fig. 4*B*). However, this reasoning cannot explain the higher W-7 conductance compared with those of W-1 and W-4, which requires considering coupling with the electrodes. Whereas the MPA linker decouples the amino acid subunits from the Au electrode at the N terminus, as is evident from the constant work functions derived from UPS, this is not the case at the C terminus. The Trp indole ring of W-7 is apparently sufficiently close to the top Au electrode to increase the interface coupling term, T_C, ∼5× compared with the other Ala-terminated peptides (*SI Appendix*, section SI-5).

The above consideration is limited to near-zero bias voltage. Extracting further, quantitative information from bias-dependent transport is problematic in practice because of the large number of unknown parameters in a full, bias-dependent version of Eq. **1** [see the supporting information of ref. 57], and rather featureless current–voltage curves. Therefore, we use as an alternative way to quantify the dual effect of Trp doping on transport along the molecule ($\sum_{i=1}^{n} -\beta_i l_i$ in Eq. **1**) and on coupling to the electrodes ($T_{C,N}$) the Landauer formula (20, 59), simplified by ignoring all transmission function features, except for one peak. The energy position of this peak, ε_0 (see the dashed line in Fig. 4 *A*, *iii*) and its Lorentzian broadening, Γ_g (the width of the peak in Fig. 4 *A*, *iii*) provide a genuine description of the transport, even though it generally combines contributions from several molecular levels. Moreover, it was shown that distinctly different tunneling models such as transmission function or multistep superexchange can be mapped on one another (60, 61), suggesting that these two effective parameters [ε_0 and Γ_g, or another pair of equivalent parameters in generic polynomial models (20, 61)] characterize the observed current–voltage relations (*SI Appendix*, section SI-3) (59):

$$I \cong N\frac{2e}{h}\Gamma_g^2\frac{eV}{(\varepsilon_0+\alpha eV)^2-(eV/2)^2}, \qquad [2]$$

where e and h are the electron charge and the Planck constant, respectively, and α measures the asymmetry of the bias partition, found to be negligible in this case. The number of molecules in the junction, N, is a known uncertainty in all but single-molecule junctions (28) ($N \sim$ 100–10,000; see *SI Appendix*, sections 3, 4), but is merely a constant: neither the quality of fit, nor ε_0 is influenced by N.

To evaluate the trends in Γ_g, the geometric average of electrode–peptide coupling ($\Gamma_g \equiv \sqrt{\Gamma_N \Gamma_C}$), we used a conservative estimate of $N = 100$. Fig. 4*C* shows that Γ_g (see *SI Appendix*, Table S3 for a full list of extracted parameters) varies as W-7 >> W-4 ∼ W-1 > 7A, and reflects most of the net change in current magnitude (Fig. 4*C*). Given the similar coupling at the N terminus (via

the MPA linker, Γ_N), coupling at the C terminus, Γ_C, must be the reason for the higher Γ_g of W-7. As noted above, the proximity of the Trp's aromatic indole side chain to the Au electrode suffices to increase Γ_g, which enhances ETp efficiency across the junction. In addition Trp doping, even at the peptide sequence center (W-1, W-4) slightly enhances Γ_g, the effective coupling term, compared with Γ_g for 7A. The 0.1–0.2-meV values of Γ_g for the peptides are rather low (even lower for $N > 100$), compared with ∼1 meV reported for similar length fully conjugated dithiol molecules (62).

The similarity in ε_0 values among the three Trp-doped peptides (compare 7A; Fig. 4*B*), despite the large difference in their net current (*SI Appendix*, Fig. S2), supports the model of Eq. **1** that transport within the peptide is roughly indifferent to sequence. Furthermore, Fig. 4*B* shows that the changes in effective energy barrier generally follow the trend that is observed in the gas-phase calculations and, from UPS results on monolayers, with ε_0 of 7A > W-4 > W-1. W-7, though, is exceptional: its low ε_0 does not follow the trend of the UPS or DFT results, or of the ε_0 values for W-1 and W-4. We postulate that for W-7 contact/overlap between the Au's spillover electron density and the indole ring's π-electrons is sufficient to decrease the effective transport barrier (63). Such sensitivity of the energy levels to mere physical proximity to the metallic contact was not observed for thiol-terminated polyphenyls (62), from another hand indicating that actual chemical bonding can act to buffer coupling, rather than enhance it, possibly via electron localization in the bond (64, 65). In addition, the separation into Γ_g and ε_0 reveals that the slightly lower current via W-4 compared with W-1 (Fig. 4*C*, red circles) is expressed as a higher energy barrier, whereas their extracted coupling values, Γ_g, are the same.

Finally, we note that the effective barrier extracted from fitting I-V data to Eq. **2** is about half the UPS energy offset, although for the nondoped 7A the difference is less. This implies that the effective barrier ε_0 differs significantly from the molecular HOMO, in contrast to previous observation (62), because ε_0 corresponds to the heterogeneous energy landscape of the transport, not only to a certain HOMO. This may reflect that transport (61) via peptides differs from that via a fully conjugated wire, where a closer match between transmission function and HOMO level was reported (62).

Conclusion

We have shown that tailoring the composition and sequence of peptides can modulate the electrical conductance of peptide junctions by adjusting the energy barrier height and electrode–peptide coupling. Adding a single Trp to 6-Ala peptide adds an HOMO level with 1–2 eV above that of the homo-Ala peptide, as revealed by DFT for isolated peptide in the gas phase. As shown by UPS, adsorbing a monolayer of such a peptide changes its molecular levels and the HOMO of the Trp-doped peptide is then only 0.5–1 eV above that of the intrinsic Ala peptide. Doping induces a heterogeneous energy barrier, and therefore charge transport is along a multisite path, described by superexchange-mediated tunneling. IETS shows that the Trp moiety is involved in the transport. Effective transport parameters can be approximated by fitting to a Lorentzian transmission function. Such fitting indicates a drastic reduction in the effective energy barrier for tunneling transport, caused by the Trp doping, of ∼1 eV, with minor dependence on the exact position of the Trp within the sequence. At the same time the Trp location is critical when it is adjacent to the electrode, as in W-7 the effective coupling term is strongly enhanced. UPS, DFT calculations, and theoretical analyses of the electrical transport results agree with the conclusion that the shape of the heterogeneous tunneling barrier and its coupling to the electrodes are drastically affected by the presence of the indole side chain. It implies that the two generic characteristics of transport by tunneling, energy barrier, and coupling can be independently engineered by the choice of amino acid and their sequence. Heterogeneous oligopeptides thus represent a versatile, readily available tool for controlled (bio)electronic applications, where peptide wires can be designed by using amino acids as building blocks.

Materials and Methods

Chemicals and Materials. Peptides with MPA linker at the N terminus were purchased from GL Biochem Ltd. and Hylabs Ltd. with purity >95% (HPLC). Peptides W-1, W-4, and W-7 were dissolved in mixed acetonitrile (ACN) and water with the ratio of 1:3 and 7A in 3:1. The concentration of all peptides in the solution was 0.25 mM.

Peptide Monolayer Preparation on Au Substrate. Au substrates were cleaned by sonication in water and ethanol for 5 min, respectively, followed by plasma etching for 5 min under a mixed flow of 1:1 Ar and O_2. The Au substrates were further treated by hot ethanol to remove the oxidized Au. After another 10-min treatment by UV/ozone, the Au substrates were incubated in peptide solution for 48 h, and were then washed with ACN:H_2O/ethanol and dried in a flow of dry nitrogen.

Current–Voltage Measurement. More than 100 junctions were recorded for statistics from 2 to 4 different macroscopic-electrode chips. The half width at half maximum for the distribution of logarithmic current at –0.5 V is about an order of magnitude. For each peptide, ∼20 junctions at the center of distribution were selected for temperature control measurement.

Further details on characterization and computation are provided in *SI Appendix*.

ACKNOWLEDGMENTS. This research was made possible in part by the historic generosity of the Harold Perlman family. We thank the Minerva Foundation (Munich), the Nancy and Stephen Grand Center for Sensors and Security, the Benoziyo Endowment Fund for the Advancement of Science, J&R Center for Scientific Research, and the Kimmelman Center for Biomolecular Structure and Assembly for partial support. S.R.-A. acknowledges an Adams Fellowship of the Israel Academy of Sciences and Humanities. L.S. thanks the Israeli Ministry of Science for an Eshkol Scholarship. L.K. acknowledges support by the European Research Council and the Israel Science Foundation. M.S. holds the Katzir-Makineni Chair in Chemistry; D.C. holds the Schaefer Chair in Energy Research.

1. Gatto E, Venanzi M (2013) Peptronics: Peptide materials for electron transfer. *Peptide Materials: From Nanostructures to Applications*, eds Alemán C, Bianco A, Venanzi M (John Wiley & Sons, Chichester, UK), pp 105–147.
2. Gray HB, Winkler JR (2003) Electron tunneling through proteins. *Q Rev Biophys* 36(3):341–372.
3. Shah A, et al. (2015) Electron transfer in peptides. *Chem Soc Rev* 44(4):1015–1027.
4. Gao J, et al. (2011) Electron transfer in peptides: The influence of charged amino acids. *Angew Chem Int Ed Engl* 50(8):1926–1930.
5. Winkler JR, Nocera DG, Yocom KM, Bordignon E, Gray HB (1982) Electron-transfer kinetics of pentaammineruthenium(III)(histidine-33)-ferricytochrome-c - measurement of the rate of intramolecular electron-transfer between redox centers separated by 15-A in a protein. *J Am Chem Soc* 104(21):5798–5800.
6. Farver O, Pecht I (1989) Long-range intramolecular electron transfer in azurins. *Proc Natl Acad Sci USA* 86(18):6968–6972.
7. Malak RA, Gao Z, Wishart JF, Isied SS (2004) Long-range electron transfer across Peptide bridges: The transition from electron superexchange to hopping. *J Am Chem Soc* 126(43):13888–13889.
8. Sek S (2013) Review: Peptides and proteins wired into the electrical circuits: An SPM-based approach. *Biopolymers* 100(1):71–81.
9. Xiao X, Xu B, Tao N (2004) Conductance titration of single-peptide molecules. *J Am Chem Soc* 126(17):5370–5371.
10. Chi QJ, et al. (2000) Molecular monolayers and interfacial electron transfer of *Pseudomonas aeruginosa* azurin on Au(111). *J Am Chem Soc* 122(17):4047–4055.
11. Sek S, Misicka A, Swiatek K, Maicka E (2006) Conductance of alpha-helical peptides trapped within molecular junctions. *J Phys Chem B* 110(39):19671–19677.
12. Wierzbinski E, et al. (2012) Effect of backbone flexibility on charge transfer rates in peptide nucleic acid duplexes. *J Am Chem Soc* 134(22):9335–9342.
13. Blumberger J (2015) Recent advances in the theory and molecular simulation of biological electron transfer reactions. *Chem Rev* 115(20):11191–11238.
14. Onuchic JN, Beratan DN, Winkler JR, Gray HB (1992) Pathway analysis of protein electron-transfer reactions. *Annu Rev Biophys Biomol Struct* 21:349–377.
15. Schlag EW, Sheu S-Y, Yang D-Y, Selzle HL, Lin SH (2007) Distal charge transport in peptides. *Angew Chem Int Ed Engl* 46(18):3196–3210.
16. Skourtis SS (2013) Review: Probing protein electron transfer mechanisms from the molecular to the cellular length scales. *Biopolymers* 100(1):82–92.
17. Winkler JR, Gray HB (2014) Long-range electron tunneling. *J Am Chem Soc* 136(8):2930–2939.

18. Facci P (2014) *Biomolecular Electronics: Bioelectronics and the Electrical Control of Biological Systems and Reactions* (William Andrew Inc., Waltham, MA), pp 1–240.
19. Wang M, Gao J, Müller P, Giese B (2009) Electron transfer in peptides with cysteine and methionine as relay amino acids. *Angew Chem Int Ed Engl* 48(23):4232–4234.
20. Cuevas J-C, Scheer E (2010) *Molecular Electronics. An Introduction to Theory and Experiment* (World Scientific, Singapore), p 724.
21. Artés JM, et al. (2012) Current-voltage characteristics and transition voltage spectroscopy of individual redox proteins. *J Am Chem Soc* 134(50):20218–20221.
22. Zhao J, Davis JJ, Sansom MSP, Hung A (2004) Exploring the electronic and mechanical properties of protein using conducting atomic force microscopy. *J Am Chem Soc* 126(17):5601–5609.
23. Sepunaru L, Friedman N, Pecht I, Sheves M, Cahen D (2012) Temperature-dependent solid-state electron transport through bacteriorhodopsin: Experimental evidence for multiple transport paths through proteins. *J Am Chem Soc* 134(9):4169–4176.
24. Sepunaru L, Pecht I, Sheves M, Cahen D (2011) Solid-state electron transport across azurin: From a temperature-independent to a temperature-activated mechanism. *J Am Chem Soc* 133(8):2421–2423.
25. Galperin M, Ratner MA, Nitzan A, Troisi A (2008) Nuclear coupling and polarization in molecular transport junctions: Beyond tunneling to function. *Science* 319(5866): 1056–1060.
26. Troisi A, et al. (2007) Tracing electronic pathways in molecules by using inelastic tunneling spectroscopy. *Proc Natl Acad Sci USA* 104(36):14255–14259.
27. Yu X, et al. (2015) Insights into solid-state electron transport through proteins from inelastic tunneling spectroscopy: The case of azurin. *ACS Nano* 9(10):9955–9963.
28. Amdursky N, et al. (2014) Electronic transport via proteins. *Adv Mater* 26(42): 7142–7161.
29. Baghbanzadeh M, et al. (2015) Charge tunneling along short oligoglycine chains. *Angew Chem Int Ed Engl* 54(49):14743–14747.
30. Ron I, Pecht I, Sheves M, Cahen D (2010) Proteins as solid-state electronic conductors. *Acc Chem Res* 43(7):945–953.
31. Maruccio G, et al. (2005) Towards protein field-effect transistors: Report and model of prototype. *Adv Mater* 17(7):816–822.
32. Sepunaru L, et al. (2015) Electronic transport via homopeptides: The role of side chains and secondary structure. *J Am Chem Soc* 137(30):9617–9626.
33. Shih C, et al. (2008) Tryptophan-accelerated electron flow through proteins. *Science* 320(5884):1760–1762.
34. Takematsu K, et al. (2013) Tryptophan-accelerated electron flow across a protein-protein interface. *J Am Chem Soc* 135(41):15515–15525.
35. Lukacs A, Eker APM, Byrdin M, Brettel K, Vos MH (2008) Electron hopping through the 15 A triple tryptophan molecular wire in DNA photolyase occurs within 30 ps. *J Am Chem Soc* 130(44):14394–14395.
36. Aubert C, Vos MH, Mathis P, Eker APM, Brettel K (2000) Intraprotein radical transfer during photoactivation of DNA photolyase. *Nature* 405(6786):586–590.
37. Wittekindt C, Schwarz M, Friedrich T, Koslowski T (2009) Aromatic amino acids as stepping stones in charge transfer in respiratory complex I: An unusual mechanism deduced from atomistic theory and bioinformatics. *J Am Chem Soc* 131(23): 8134–8140.
38. Noy G, Ophir A, Selzer Y (2010) Response of molecular junctions to surface plasmon polaritons. *Angew Chem Int Ed Engl* 49(33):5734–5736.
39. Barth A (2000) The infrared absorption of amino acid side chains. *Prog Biophys Mol Biol* 74(3-5):141–173.
40. Mirjani F, Thijssen JM, Whitesides GM, Ratner MA (2014) Charge transport across insulating self-assembled monolayers: Non-equilibrium approaches and modeling to relate current and molecular structure. *ACS Nano* 8(12):12428–12436.
41. Jaklevic RC, Lambe J (1966) Molecular vibration spectra by electron tunneling. *Phys Rev Lett* 17(22):1139–1140.
42. Kushmerick JG, et al. (2004) Vibronic contributions to charge transport across molecular junctions. *Nano Lett* 4(4):639–642.
43. Sepunaru L (2015) Building block towards systematic bioelectronics. PhD thesis (Feinberg Graduate School of Weizmann Institute of Science, Rehovot, Israel).
44. Beebe JM, Moore HJ, Lee TR, Kushmerick JG (2007) Vibronic coupling in semi-fluorinated alkanethiol junctions: Implications for selection rules in inelastic electron tunneling spectroscopy. *Nano Lett* 7(5):1364–1368.
45. Okabayashi N, Paulsson M, Ueba H, Konda Y, Komeda T (2010) Site selective inelastic electron tunneling spectroscopy probed by isotope labeling. *Nano Lett* 10(8): 2950–2955.
46. Quek SY, Choi HJ, Louie SG, Neaton JB (2011) Thermopower of amine-gold-linked aromatic molecular junctions from first principles. *ACS Nano* 5(1):551–557.
47. Eckshtain-Levi M, et al. (2016) Cold denaturation induces inversion of dipole and spin transfer in chiral peptide monolayers. *Nat Commun* 7:10744.
48. Egger DA, et al. (2014) Outer-valence electron spectra of prototypical aromatic heterocycles from an optimally tuned range-separated hybrid functional. *J Chem Theory Comput* 10(5):1934–1952.
49. Refaely-Abramson S, et al. (2012) Quasiparticle spectra from a nonempirical optimally tuned range-separated hybrid density functional. *Phys Rev Lett* 109(22):226405.
50. Neaton JB, Hybertsen MS, Louie SG (2006) Renormalization of molecular electronic levels at metal-molecule interfaces. *Phys Rev Lett* 97(21):216405.
51. Rissner F, et al. (2011) Collectively induced quantum-confined Stark effect in monolayers of molecules consisting of polar repeating units. *J Am Chem Soc* 133(46): 18634–18645.
52. Heimel G, Romaner L, Brédas JL, Zojer E (2006) Interface energetics and level alignment at covalent metal-molecule junctions: Pi-conjugated thiols on gold. *Phys Rev Lett* 96(19):196806.
53. Toledano T, et al. (2015) Effect of binding group on hybridization across the silicon/aromatic-monolayer interface. *J Electron Spectrosc* 204:149–158.
54. Van Dyck C, Geskin V, Cornil J (2014) Fermi level pinning and orbital polarization effects in molecular junctions: The role of metal induced gap states. *Adv Funct Mater* 24(39):6154–6165.
55. Beratan DN, Betts JN, Onuchic JN (1991) Protein electron transfer rates set by the bridging secondary and tertiary structure. *Science* 252(5010):1285–1288.
56. Kawatsu T (2013) Review: Pathway analysis for peptide-mediated electronic coupling in the super-exchange mechanism of ET and EET. *Biopolymers* 100(1):100–113.
57. Liao K-C, Hsu L-Y, Bowers CM, Rabitz H, Whitesides GM (2015) Molecular series-tunneling junctions. *J Am Chem Soc* 137(18):5948–5954.
58. Lee C, Mertz B (2016) Theoretical evidence for multiple charge transfer pathways in Bacteriorhodopsin. *J Chem Theory Comput* 12(4):1639–1646.
59. Baldea I (2012) Ambipolar transition voltage spectroscopy: Analytical results and experimental agreement. *Phys Rev B* 85(3):035442.
60. Holmlin RE, et al. (2001) Correlating electron transport and molecular structure in organic thin films. *Angew Chem Int Ed Engl* 40(12):2316–2320.
61. Vilan A, Cahen D, Kraisler E (2013) Rethinking transition voltage spectroscopy within a generic Taylor expansion view. *ACS Nano* 7(1):695–706.
62. Xie Z, Bâldea I, Smith CE, Wu Y, Frisbie CD (2015) Experimental and theoretical analysis of nanotransport in oligophenylene dithiol junctions as a function of molecular length and contact work function. *ACS Nano* 9(8):8022–8036.
63. Busiakiewicz A, et al. (2010) Electronic transport properties of individual 4,4′-bis(mercaptoalkyl)-biphenyl derivatives measured in STM-based break junctions. *Phys Chem Chem Phys* 12(35):10518–10524.
64. Akkerman HB, de Boer B (2008) Electrical conduction through single molecules and self-assembled monolayers. *J Phys-condens Mat* 20(1):013001.
65. Yelin T, et al. (2016) Conductance saturation in a series of highly transmitting molecular junctions. *Nat Mater* 15(4):444–449.